

# We are IntechOpen, the world's leading publisher of Open Access books Built by scientists, for scientists

6,900

Open access books available

185,000

International authors and editors

200M

Downloads

Our authors are among the

154

Countries delivered to

TOP 1%

most cited scientists

12.2%

Contributors from top 500 universities



WEB OF SCIENCE™

Selection of our books indexed in the Book Citation Index  
in Web of Science™ Core Collection (BKCI)

Interested in publishing with us?  
Contact [book.department@intechopen.com](mailto:book.department@intechopen.com)

Numbers displayed above are based on latest data collected.  
For more information visit [www.intechopen.com](http://www.intechopen.com)



## Anodization of Magnesium Alloys Using Phosphate Solution

Koji Murakami<sup>1</sup>, Makoto Hino<sup>1</sup> and Teruto Kanadani<sup>2</sup>

<sup>1</sup>Industrial Technology Research Institute of Okayama Prefectural Government

<sup>2</sup>Okayama University of Science

<sup>1,2</sup>Japan

### 1. Introduction

Magnesium alloys are increasingly utilized recently to improve fuel consumption of vehicles by reducing their weight. Suppression of oscillation, shielding of electromagnetic wave, rigidity and recyclability of the alloys are also advantages in electric and electronic products as well as in automotive applications (Cole, 2003). However, magnesium is one of the materials which bear stain most easily because of its quite low potential region where metallic magnesium can exist in wet environment (Pourbaix, 1974; Mears & Brown, 1945) (Fig. 1).

As protective coatings for magnesium alloys, conventional anodizations by Dow17 and HAE (Evangelides, 1955; Company, 1956; 1981; 1998; Ono & Masuko, 2003) treatments have successfully been utilized, but these methods require harmful chemical agents such

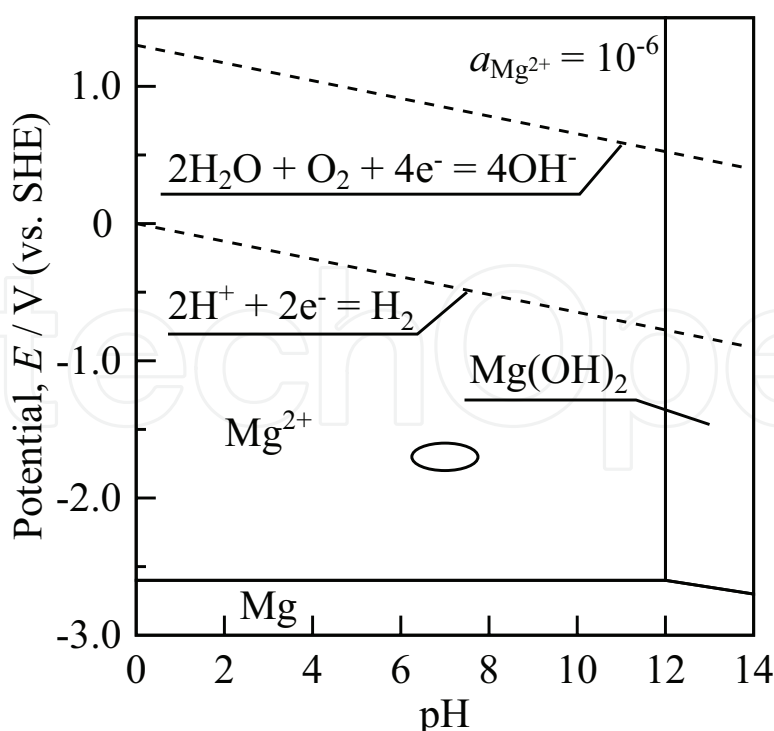


Fig. 1. Potential-pH diagram of magnesium-water system (Pourbaix, 1974; Mears & Brown, 1945) (circled area shows rest potential).

as chromium oxide (VI) and fluoride which have recently been restricted by the RoHS (Restriction of the use of certain Hazardous Substances in electrical and electronic equipment) directive and current trend for reducing environmental load. Another protection of magnesium alloys by anodization is performed using phosphate solution (Barton, 1998; Saijo et al., 2005; Murakami et al., 2007; Hino et al., 2007; Murakami et al., 2008; Saijo et al., 2008; Hino et al., 2008) whose electrolyte consists of phosphate and ammonium salt. Because of the simple electrolyte for the anodization, its environmental load is quite lighter compared with those of Dow17 and HAE.

The main purpose of this chapter is to clarify the microstructures and mechanisms of corrosion protection on the anodized surfaces by elucidating the differences in modes of protections. In section 2, formation of anodized layer through electrolysis in phosphate solution with electric discharge is discussed by microstructural observation. Mechanisms of corrosion protection on the anodized surfaces are clarified in section 3 by electrochemical measurements and microscopy.

2. Microstructure of anodized layer

2.1 Experimental

Die-cast plates of ASTM AZ91D (Mg-9.1Al-0.75Zn) magnesium alloy, rolled sheets of AZ31B (Mg-2.9Al-0.85Zn) magnesium alloy and cast high-purity magnesium (99.95 mass%) were used as substrates. Here, high-purity magnesium is designated as ‘3N-Mg’ in the following sentences. Chemical compositions of the substrates are shown in Table 1. After the substrates were degreased and etched in a potassium hydroxide solution and a phosphate solution, respectively, they were anodized either in Dow17 (Company, 1956; 1981; 1998; Ono & Masuko, 2003) or in phosphate electrolyte (Barton, 1998; Saijo et al., 2005; Murakami et al., 2007; Hino et al., 2007; Murakami et al., 2008; Saijo et al., 2008; Hino et al., 2008). The electrolysis in phosphate solution was carried out by using a commercial solution (Anomag CR1 and CR2, Henkel Japan Co., Ltd.) according to its instruction. The counter electrodes were plates of stainless steel (JIS SUS316L or AISI 316L) which face both surfaces of the specimen, and the temperature of the electrolyte was 298±5 K. The mode of electrolysis in the phosphate solution can be DC (direct current) or AC (alternating current) (Saijo et al., 2008), but only DC electrolysis is discussed in this chapter.

Figure 2 shows the appearance of the specimen during anodization. After initiation of electrolysis, the surface of the specimen was covered with an anodized layer whose color turned to white within a few seconds. The amount of gas generated on the surface increased with the growth of the anodized layer (Fig. 2(a)), and the surface was then covered with a visible local discharge or sparks when the bias reached 200 V (Fig. 2(b)). Thickness of anodized layer was changed by varying the bias at which an electrolysis was terminated.

The anodized specimens underwent electron probe microanalysis (EPMA) and transmission electron microscopy (TEM). X-ray diffraction patterns on the anodized surfaces were taken under Seemann-Bohlin geometry of the incident angle  $\omega=1^\circ$  with parallel beam optics (wavelength  $\lambda_{CuK\alpha}=0.1542$  nm). The specimens for cross-sectional observation and elemental

substrate	Al	Mn	Zn	Si	Cu	Ni	Fe	Mg
AZ91D	9.1	0.28	0.75	0.05	0.025	0.001	0.004	bal.
AZ31B	2.87	0.38	0.85	0.014	0.0004	0.0003	0.003	bal.
3N-Mg	0.003	0.002	0.003	0.004	<0.001	<0.001	0.002	>99.95

Table 1. Chemical compositions of substrates (in mass%).

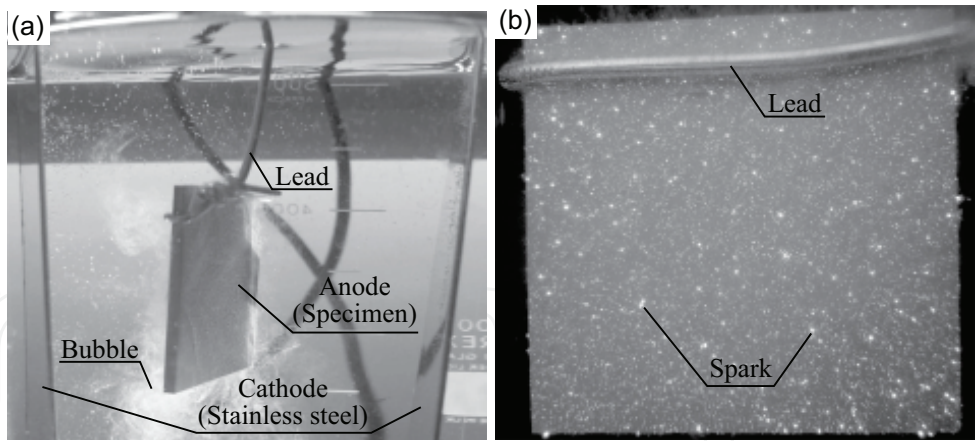


Fig. 2. Appearance of specimen during anodization ((a) immediately after initiation of electrolysis, (b) sparks on substrate).

analysis were prepared by using argon ion beam (acceleration voltage 5 kV). The surfaces were coated by epoxy resin for protection of the anodized layers before argon ion etching. Electron probe microanalysis (EPMA) with wavelength-dispersive X-ray spectrometer was used for elemental analysis. Hereafter, a specimen of AZ91D anodized in the phosphate solution, whose thickness of the anodized layer is 5  $\mu\text{m}$ , is designated as ‘AZ91D-phosphate-5 $\mu\text{m}$ ’ for simplicity.

2.2 Experimental results

Figure 3 shows the X-ray diffraction patterns taken from the anodized surfaces on AZ91D, AZ31B and 3N-Mg. The surface of AZ91D-Dow17 (Fig. 3(a)) shows chromium oxide ( $\text{Cr}_2\text{O}_3$ ),

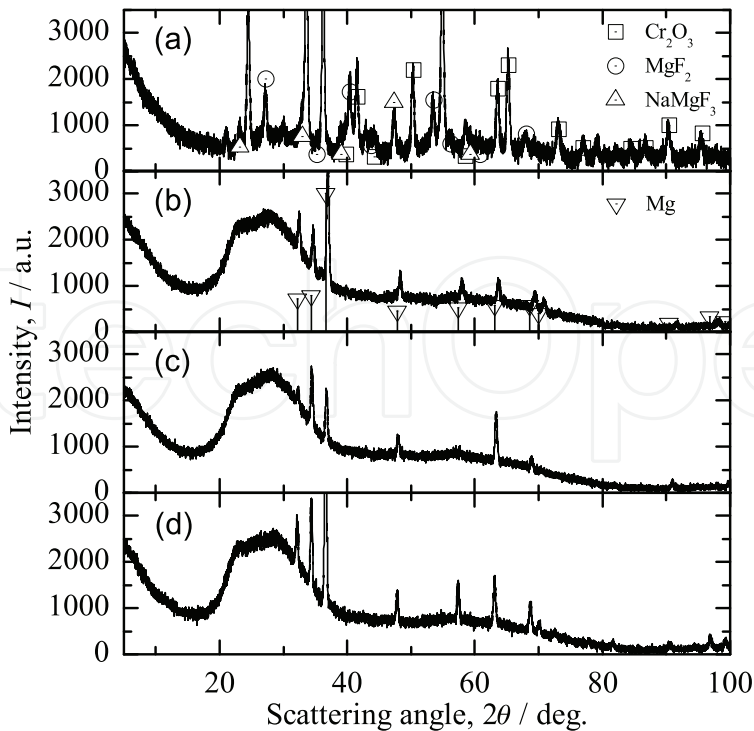


Fig. 3. X-ray diffraction patterns taken from the anodized surfaces ((a) AZ91D-Dow17, (b) AZ91D-phosphate-10 $\mu\text{m}$ , (c) AZ31B-phosphate-10 $\mu\text{m}$ , (d) 3N-Mg-phosphate-10 $\mu\text{m}$ ).

magnesium fluoride ( $\text{MgF}_2$ ) and sodium magnesium fluoride ( $\text{NaMgF}_3$ ) as crystalline substances. On the other hand, those in AZ91D/AZ31B/3N-Mg-phosphate-10 $\mu\text{m}$  show broad scattering peaks at  $20^\circ < 2\theta < 40^\circ$  (Fig. 3(b)-(d)), and the overlying peaks indicate the magnesium matrix of the substrates.

Figure 4 shows the cross-sectional microstructure of the anodized surfaces and concentrations of oxygen, magnesium, aluminum and phosphorus in the anodized layers on AZ91D/AZ31B/3N-Mg-phosphate-10 $\mu\text{m}$  obtained by EPMA. Most of the pores in the anodized layer of AZ91D-Dow17 (Fig. 4(a)) were filled with epoxy resin used for the sample preparation, and many paths were formed linking the surface and the substrate. Figures 4(b)-(f) also show porous structures in the anodized layers. The atomic ratio of the elements in the anodized layers is shown in Fig. 4(g), where atomic percent of oxygen varies from 50 to 70 at.% and that of phosphorus from 10 to 20, depending on substrate.

Figure 5 shows the bright- and dark-field images of the fragment of the anodized layer of AZ91D-phosphate-20 $\mu\text{m}$ . Although there was no characteristic microstructure in the fragment at the beginning of the TEM observation, some areas were damaged by a few seconds' irradiation of electron beam to form bubbles or show swelling. The selected area diffraction pattern taken from the dotted rectangular area in Fig. 5(a) consisted of a strong halo ring, weak Debye rings and diffraction spots. The Debye rings and the diffraction spots matched those of spinel ( $\text{MgAl}_2\text{O}_4$ ), and the dark-field image (Fig. 5(b)) taken using a diffraction spot of spinel including a part of the Debye rings showed particles of  $10^1$ - $10^2$  nm in size. Debye rings of magnesium oxide ( $\text{MgO}$ ) were also observed in other fragments, but the rings were diffuser than those of spinel.

### 2.3 Discussions

As Figs. 3, 4 and 5 show, the anodized layers obtained in phosphate electrolyte mainly consist of amorphous matrix and fine crystallites of spinel and magnesium oxide. Although the anodized layer obtained in Dow17 mainly shows crystalline substances, the layer might contain amorphous magnesium oxide which could not be clearly detected by XRD. Anodizing current at the electrolysis is due to continuing local discharges on the surface covered by insulator or anodized film. Substrate as well as anodized layer, melted by spark due to discharge during anodization, are considered to be solidified rapidly, forming amorphous-based layer which contain small crystallites of spinel, magnesium oxide and spherical or irregularly shaped pores. Anions in the electrolyte which are attracted at the anodized surface during electrolysis are mainly hydroxide ions and phosphates ( $\text{PO}_4^{3-}$ ). Phosphorus detected by EPMA in the anodized layers (Fig. 4(g)) is picked up during solidification, and the spherical pores are thought to be filled by oxygen gas which has been generated by oxidation of hydrogen in hydroxide ions ( $4\text{OH}^- \rightarrow 2\text{H}_2\text{O} + \text{O}_2 + 4\text{e}^-$ ). This mode of local discharge, which is accompanied by rapid solidification and formation of an anodized layer, is thought to reach a steady state in a period at a given bias, which determines the amount or the thickness of the anodized layer.

The formation of the anodized layer in the phosphate solution can qualitatively be understood by solidification of molten magnesium oxide which contains aluminum. Figure 6 shows the binary phase diagram of  $\text{MgO}$ - $\text{Al}_2\text{O}_3$  system (Osborn, 1953; Bansal & Heuer, 1974). According to the concentration of aluminum (Fig. 4(e)), the bulk composition is roughly at the broken line, and the anodized layers consist of magnesium oxide and spinel if crystallization thoroughly occurs during the solidification. That mode of solidification is considered to occur in another anodization (Liang et al., 2005), where magnesium oxide and spinel are



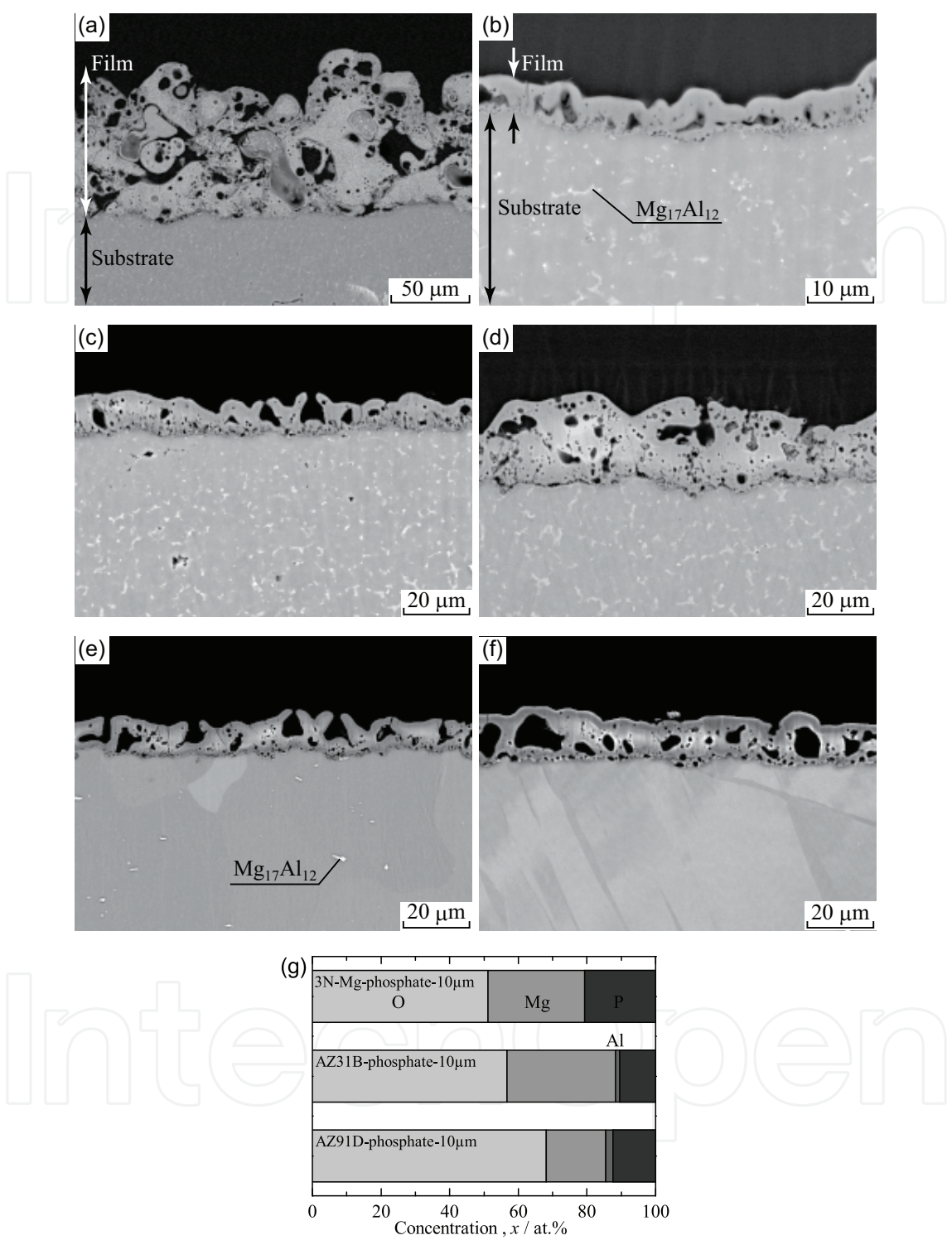


Fig. 4. Cross-sectional backscattered electron images and compositions of the anodized layers ((a) AZ91D-Dow17, (b) AZ91D-phosphate-5μm, (c) AZ91D-phosphate-10μm, (d) AZ91D-phosphate-20μm, (e) AZ31B-phosphate-10μm, (f) 3N-Mg-phosphate-10μm, (g) Compositions of the anodized layers).

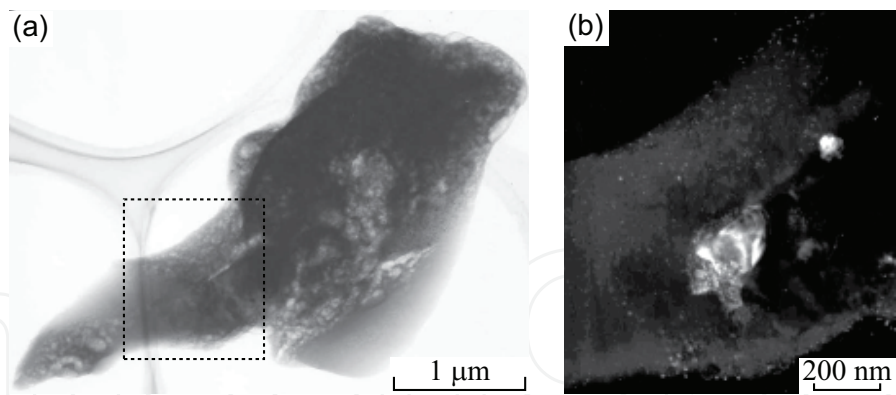


Fig. 5. Transmission electron micrographs of a fragment of anodized layer in AZ91D-phosphate-20μm ((a) Bright-field image, (b) Magnified dark-field image of the dotted rectangular area in (a)).

detected by X-ray diffraction measurements. On the other hand, those substances are only confirmed by TEM observation in this case, and the main portion of the anodized layer is amorphous (Bonilla et al., 2002).

The difference might be due to the amount of phosphorus in the electrolyte, which modifies the liquidus lines of the system and brings supercooled liquid. During the solidification, magnesium oxide firstly precipitates in the liquid, then, some portion of the supercooled liquid decomposes into fine crystallites of magnesium oxide and spinel. However, most of the supercooled liquid is considered to solidify in amorphous state because of the large cooling rate in the electrolyte. Since  $Mg_{17}Al_{12}$  phase in the substrate contains large amount of aluminum, aluminum concentration is locally higher than the dotted line in Fig. 6. In that case, spinel firstly precipitates from the liquid, and rather coarse crystallites in Fig. 5(b) are considered to have formed through this process.

By assuming that valences of oxygen, magnesium, aluminum and phosphorus are 2, 2, 3 and 5,

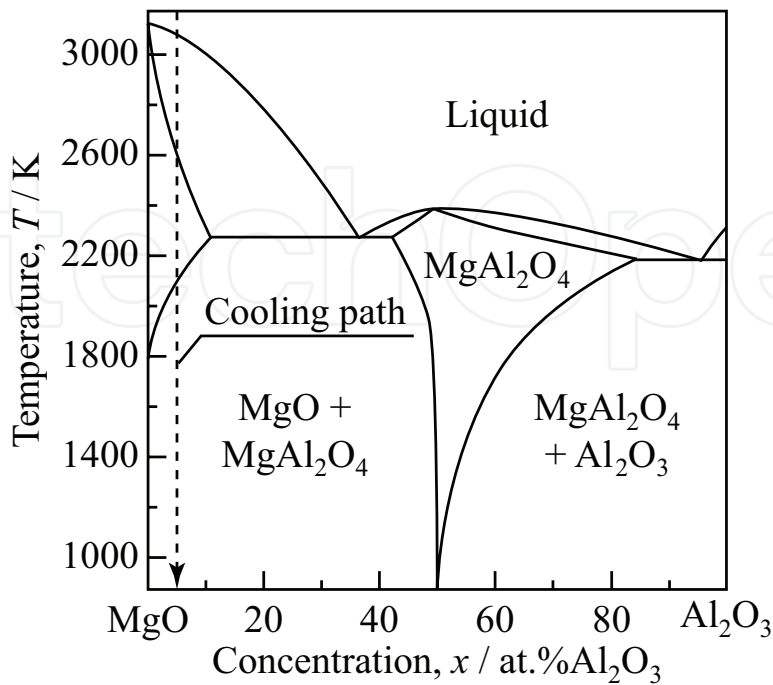


Fig. 6. Binary phase diagram of MgO- $Al_2O_3$  system (Osborn, 1953; Bansal & Heuer, 1974).

respectively, composition of the anodized layers in the case of AZ91D is roughly expressed as  $(\text{MgO})_x(\text{MgAl}_2\text{O}_4)_{17-x}(\text{Al}_2\text{O}_3)_{x-16}(\text{P}_2\text{O}_5)_{6.5}$  from Fig. 4(g). The summed amount of oxygen in this chemical formula is 52.5 which is less than the measured value 68, and the gap is thought to be due to water molecules picked up in the anodized layer. Here, elements of oxygen, magnesium, aluminum and phosphorus do not necessarily form the above stoichiometric compounds which have long-range order to show sharp peaks for X-ray diffraction, but the elements in the amorphous anodized layer are assumed to be close to these compounds in terms of short-range order.

The same discussion shows  $(\text{MgO})_x(\text{MgAl}_2\text{O}_4)_{32-x}(\text{Al}_2\text{O}_3)_{x-31.5}(\text{P}_2\text{O}_5)_5$  for AZ31B and  $(\text{MgO})_{28}(\text{P}_2\text{O}_5)_{10.5}$  for 3N-Mg. In these cases, the summed amount of oxygen is 58.5 and 80.5, respectively, while the measured values are 57 and 51. The difference, in which oxygen is calculated to be excessive according to the above assumption, is considered to be due to an inappropriate assumption for the valences of magnesium or phosphorus. That is, chemical state for each element should be  $\text{MgO}_{1-\delta}$  or  $\text{PO}_{2.5-\epsilon}$ .

### 3. Corrosion protection by anodized layer

#### 3.1 Experimental

After anodization by the above procedures, the specimens underwent salt spray test (SST, JIS Z2371 or ASTM B-117) and electrochemical measurements for assessing corrosion protectivity of the anodized surfaces. Part of the anodized specimens had their surfaces trenched by ceramic knife, then the corrosion behavior of the exposed areas in the environment of SST was examined by optical and electron microscopies. Electrochemical properties of the anodized layers were evaluated by linear sweep voltammetry (LSV) or by monitoring corrosion current at constant potential (CP). The electrolyte was a solution of 5 mass% sodium chloride whose pH was 6.5, the counter electrode was a plate of titanium coated with platinum, the reference electrode was a standard calomel electrode (SCE) with a saturated solution of potassium chloride, and each working electrode had a square window of  $25 \times 25 \text{ mm}^2$ . The rate of potential sweep was 1 mV/s in the measurement of LSV, and the potential was -1.4 V vs. SCE in CP.

For qualitative assessment of the formation of magnesium phosphate layer on the substrate due to the changes of the anodized layer in wet environment, 3N-Mg was pickled by phosphoric acid, then, immersed in solutions of trisodium phosphate dodecahydrate ( $\text{Na}_3\text{PO}_4 \cdot 12\text{H}_2\text{O}$ ) of pH 3, 7 or 11 for 30 s at 298 K. Here, the pH of each solution was set by adding phosphoric acid to the solution of trisodium phosphate dodecahydrate whose concentration was originally  $100 \text{ kg/m}^3$ . Here, the concentration of phosphate is based on a conventional conversion treatment which utilizes manganese phosphate (Hawke & Albright, 1995).

#### 3.2 Experimental results

##### 3.2.1 Salt spray test

Figure 7 shows the anodized surfaces of AZ91D after SST of 0, 518 and 2160 ks. Although corrosion products were observed locally on the surface of AZ91D-Dow17 as indicated by the broken circles, the anodized layer itself was kept as it had been before SST even in the areas surrounding the corrosion products. On the other hand, the surface of AZ91D-phosphate-10  $\mu\text{m}$  was free from visible corrosion products and had only slight discoloration on the entire surface. In the magnified optical images of the discolored surfaces,




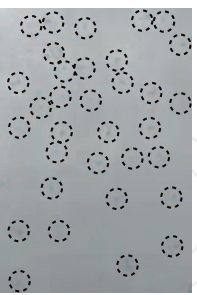
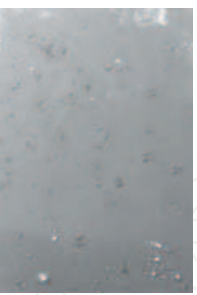
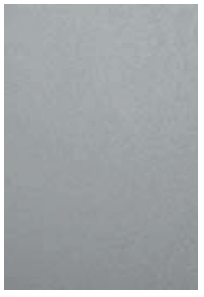


Time [ks]	0	518	2160
Dow 17			
Phosphate 10 μm			

Fig. 7. Anodized surfaces of AZ91D after salt spray test (Circles in AZ91D-Dow17-518ks indicate corrosion products, and lighter areas enclosed by broken curves in AZ91D-phosphate-10μm-2160ks correspond to reduction in anodized layer).

those areas showed local disappearance of the anodized layers especially inside the broken curves, but no remarkable corrosion product was found on those areas.

Figure 8 shows the corrosion product on the as-cast surface after salt spray test for 86.4 ks. Corrosion products with layered structure (Fig. 8(a)) were found locally on the surface, and they were identified mainly as magnesium hydroxide by X-ray diffraction (Fig. 8(b)).

Figures 9, 10, 11, 12 and 13 show the trenched areas on the anodized surfaces after SST. Since the trenched areas were not protected by anodized layers and the substrates were exposed to the wet environment containing chloride ion, the area became a starting point of corrosion in the case of AZ91D-Dow17 as shown in Fig. 9. On the other hand, Fig. 10 shows no

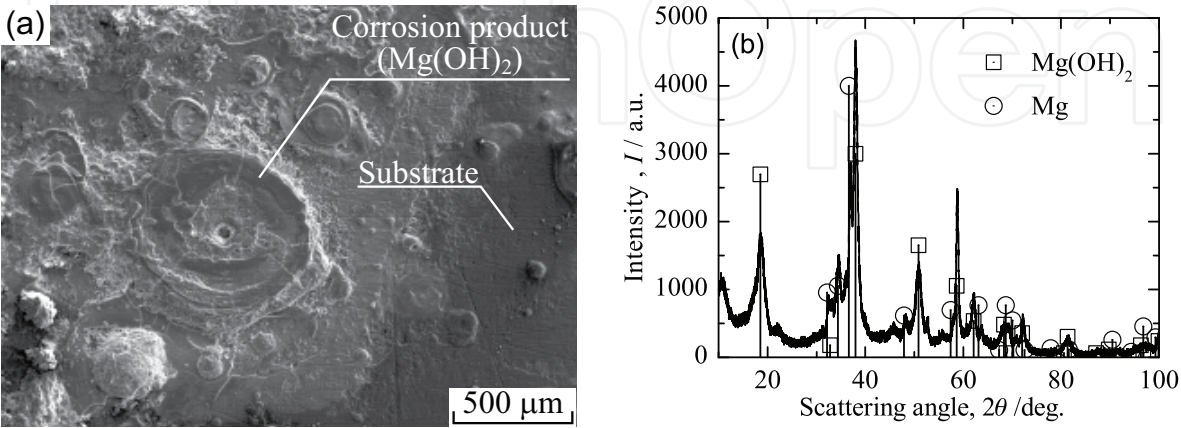


Fig. 8. Corrosion product on the as-cast AZ91D after salt spray test for 86.4 ks ((a) Secondary electron image, (b) X-ray diffraction pattern).

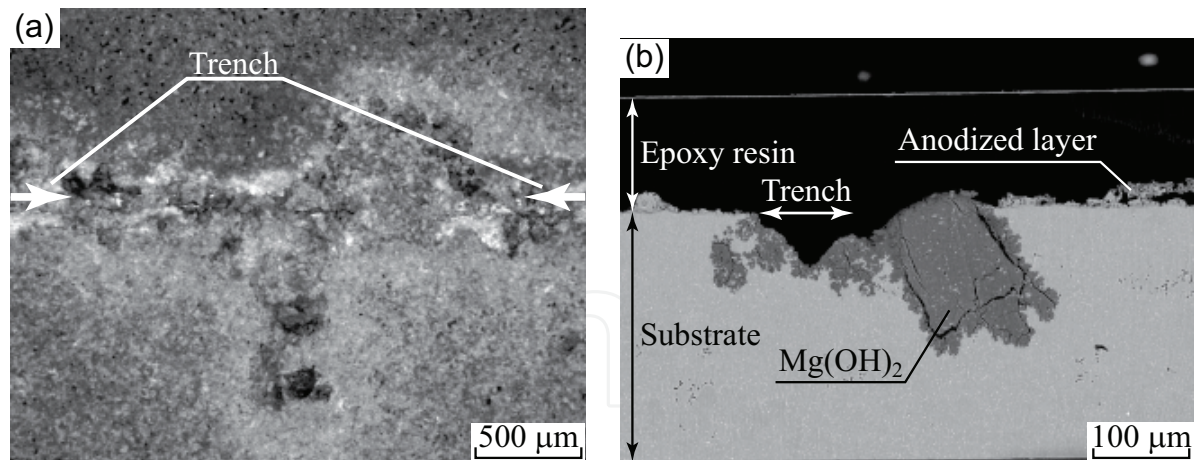


Fig. 9. Trenched surface of AZ91D-Dow17 after salt spray test for 1990 ks ((a) Optical image, (b) Cross-sectional backscattered electron image).

remarkable corrosion product (magnesium hydroxide) even in the trenched area, and cracked films were newly formed on the trenched surfaces during the test which consist of oxygen, magnesium and phosphorus (Figs. 11, 12 and 13). In the cases of AZ91D-phosphate-10μm and AZ31B-phosphate-10μm, aluminum was also contained in the regenerated film. Figure 14 shows the anodized surfaces of AZ91D-phosphate-10μm after SST for 346 ks and 1990 ks. The original anodized surface with porous morphology was kept locally after SST for 346 ks (Fig. 14(a)). Intensities of O- $K\alpha$  and P- $K\alpha$  characteristic X-rays are comparable on the original porous areas and many parts of the flat ones which lost the original morphology (Fig. 14(b),(d)). This indicates that anodized layer still remains on those areas despite the change in morphology, but most of the anodized layer was lost on the areas where the intensity of Mg- $K\alpha$  remarkably increases in Fig. 14(c). However, the morphology of the surface drastically changed after SST for 1990 ks, showing cracked areas (dark areas in Fig. 14(e)) and flat areas with less cracks (bright areas in Fig. 14(e)). Intensities of O- $K\alpha$  and P- $K\alpha$  characteristic X-rays are higher on the small fragments of ~10 μm in size which exist in the cracked areas of Fig. 14(e) than on the flat areas which seem to have lost the fragments.

3.2.2 Electrochemical properties

Figure 15 shows the polarization curves of the raw and the anodized (phosphate) surfaces obtained by LSV in 5 mass% sodium chloride solution. Anodization can successfully suppress the anodic current or corrosion rate for each substrate, and each corrosion potential is shifted

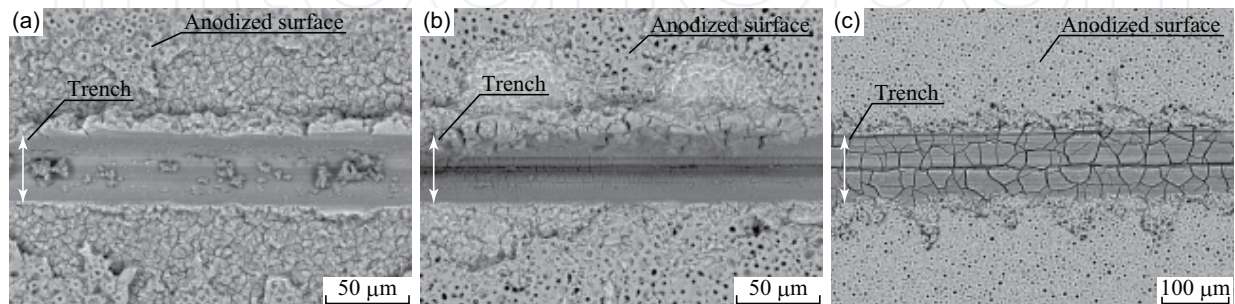


Fig. 10. Backscattered electron images of the trenched areas on the anodized surfaces after salt spray test for 605 ks ((a) AZ91D-phosphate-10μm, (b) AZ31B-phosphate-10μm, (c) 3N-Mg-phosphate-10μm).

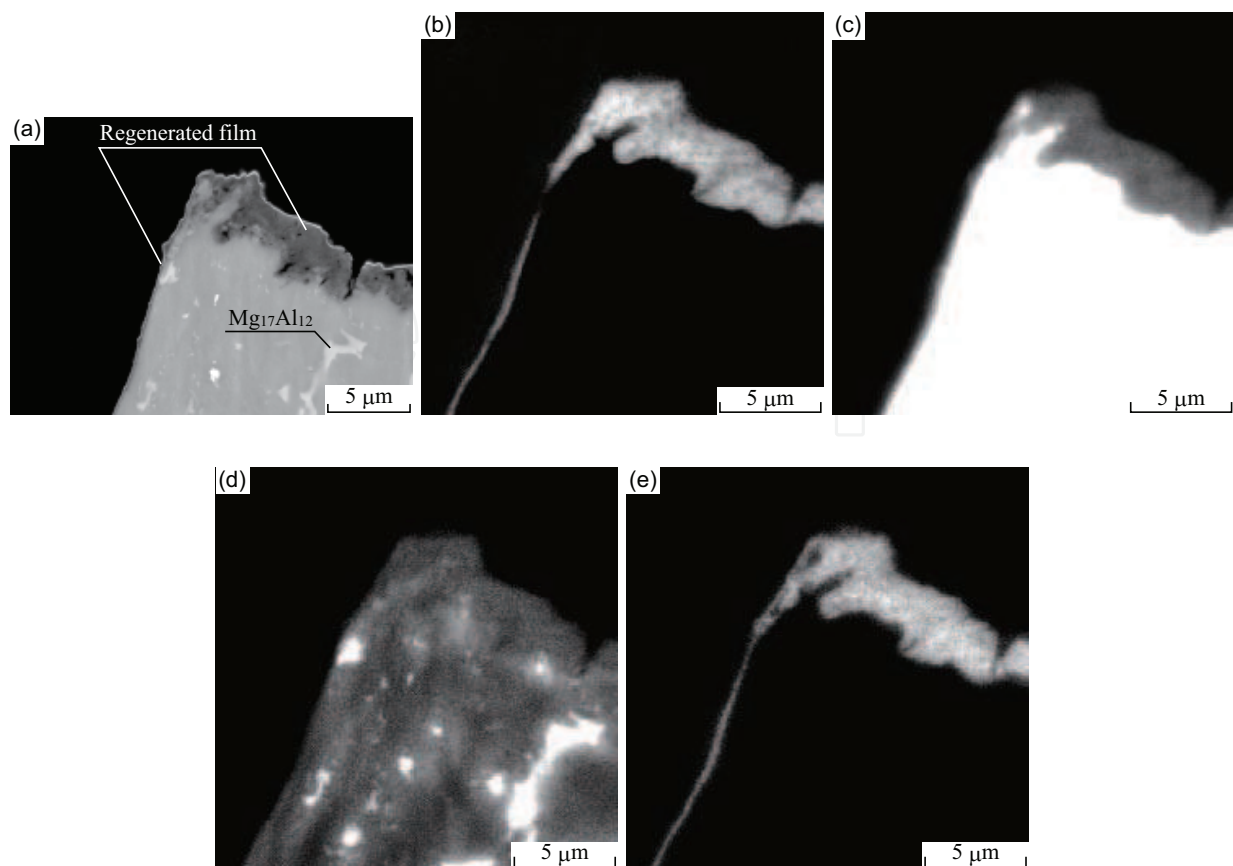


Fig. 11. Cross-sectional analyses of the trenched area on AZ91D-phosphate-10 $\mu$ m after salt spray test for 605 ks ((a) Backscattered electron image, (b) Intensity map of O-K $\alpha$  characteristic X-ray, (c) Mg-K $\alpha$ , (d) Al-K $\alpha$ , (e) P-K $\alpha$ ).

to less noble side by 150-200 mV compared with that of the untreated substrate. The anodized surfaces showed local corrosion as the potential proceeded into the anodic side.

Figure 16 shows the temporal change in current density on AZ91D-Dow17 and AZ91D-phosphate-20 $\mu$ m held at a constant potential of -1.4 V (vs. SCE) in 5 mass% sodium chloride solution. While the anodic current rapidly increased immediately after the beginning of the measurement in the case of AZ91D-Dow17, AZ91D-phosphate-20 $\mu$ m showed a plateau where anodic current density was  $\sim 10^{-2}$  A/m<sup>2</sup> before the substrate began to show local corrosion and hydrogen gas was correspondingly generated. After these electrochemical measurements, the cross section of AZ91D-Dow17 showed corrosion of the substrate above which an anodized layer still remained. On the other hand, corrosion of the substrate was observed only beneath the areas where the anodized layer disappeared in the case of AZ91D-phosphate-20 $\mu$ m.

Figure 17 shows the surface morphology of 3N-Mg after immersion into the trisodium phosphate solutions. The treatment by the solution of pH = 11 (Fig. 17(d)) showed no visible reaction on the substrate which resulted in almost the same surface as that obtained by pickling (Fig. 17(a)), and the treatment by the solution of pH = 3 (Fig. 17(b)) resulted in intense dissolution of the substrate. On the other hand, the solution of pH = 7 brought about precipitation of salt and its resulting local coating on the substrate.



3.3 Discussions

Figures 7, 9, 10, 11, 12 and 13 show that the mechanism of corrosion protection is largely different between the case of Dow17 and that of anodization in phosphate electrolyte. Since paths exist in the porous anodized layer (Dow17) which link the substrate and the surface, corrosion begins at the points where the substrate contacts water which infiltrates from the surface within 500 ks after the initiation of SST. From the point that the anodized layer obtained in Dow17 was kept as it had been after the anodization even at the areas which surround the corrosion products (Fig. 7), its mode of corrosion protection is close to that by tin plating on iron, where red rust is brought immediately by defects or damages on the plated surface which expose iron substrate.

On the other hand, the discoloration of AZ91D-phosphate-10μm in Fig. 7 does not correspond to formation of magnesium hydroxide (Fig. 8), but to disappearance of the original anodized layer (Fig. 14). The areas are thought to be anodic sites where the anodized layer dissolves into sodium chloride solution during salt spray test. The morphology of the anodized layers on AZ91D-phosphate-10μm changed from porous one (Fig. 4) to cracked one (Fig. 14(e)-(h)) during SST. The cracked areas are similar to the newly formed surfaces (Fig. 10) in the trenched area, and their morphology is also similar to that obtained by conversion coating which utilizes phosphate solution (Hawke & Albright, 1995). This mode of corrosion well suppresses intense corrosion of magnesium alloys or formation of magnesium hydroxide.

Although the anodized layers obtained in phosphate electrolyte are electrochemically less noble than the substrate, Figs. 15 and 16 show its dissolving rate into water or corrosion rate is quite low (Cai et al., 2006). Increase in thickness of the anodized layer is thought to correspond to the enlargement in the range of sacrificial protection, which means elongated duration in practical use. That is, corrosion protectivity is maintained even on the areas where the original anodized layer is mechanically lost, as long as the remaining one nearby

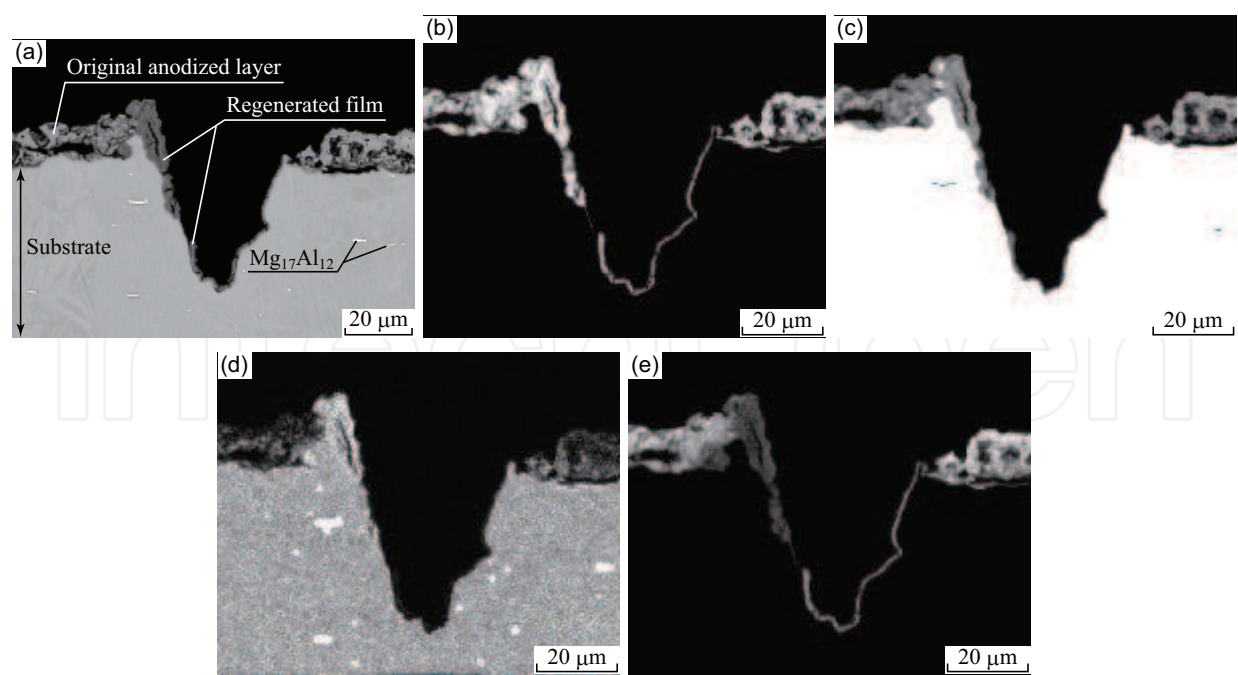


Fig. 12. Cross-sectional analyses of the trenched area on AZ31B-phosphate-10μm after salt spray test for 605 ks ((a) Backscattered electron image, (b) Intensity map of O-Kα characteristic X-ray, (c) Mg-Kα, (d) Al-Kα, (e) P-Kα).

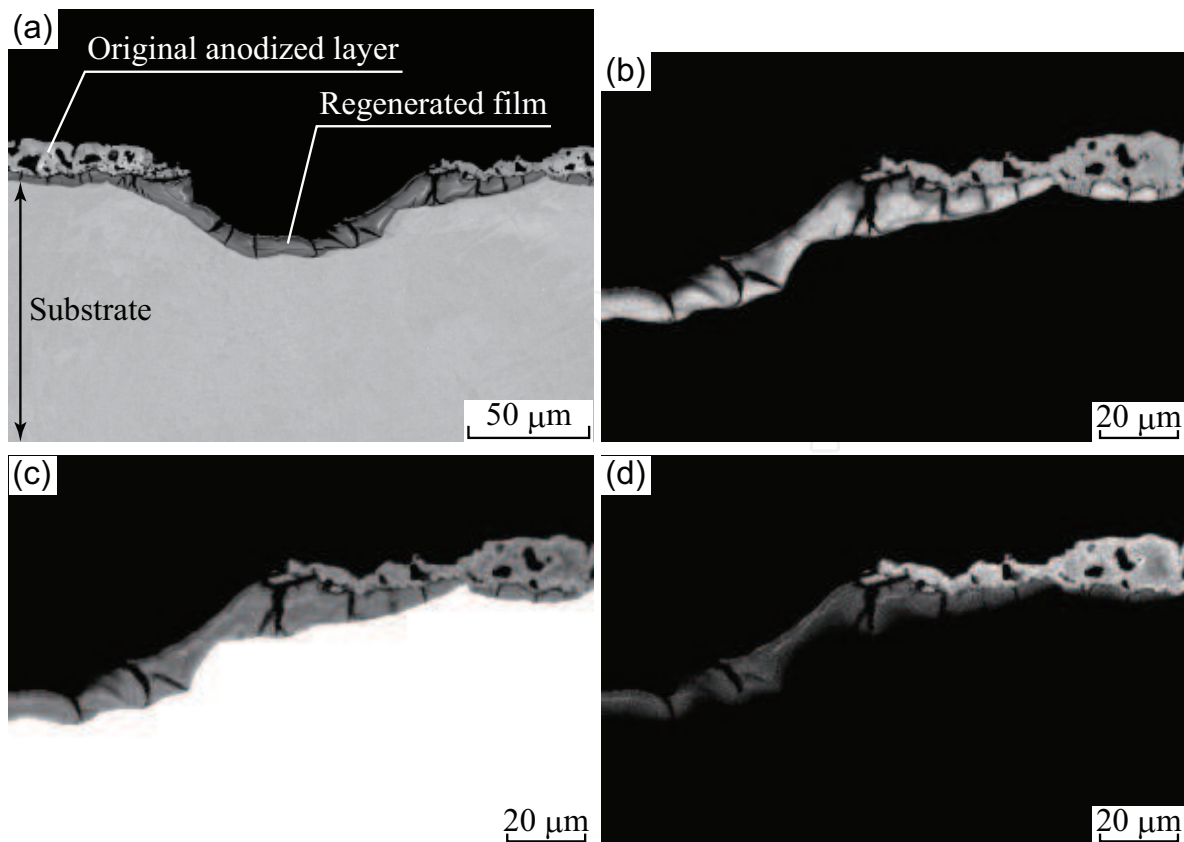


Fig. 13. Cross-sectional analyses of the trenched area on 3N-Mg-phosphate-10 $\mu$ m after salt spray test for 605 ks ((a) Backscattered electron image, (b) Intensity map of O- $K\alpha$  characteristic X-ray, (c) Mg- $K\alpha$ , (d) P- $K\alpha$ ).

can provide the components required for the formation of another protective layer observed in Figs. 11, 12, 13 and 14(e)-(h). In addition to the sacrificial protection (thermodynamics) and the low dissolving rate (kinetics) of the anodized layer obtained in phosphate electrolyte, the wet environment containing dissolved components as phosphate, which have originally existed in the anodized layer, is considered to have an appropriate pH and work as a solution for conversion treatment to form another protective layer on the substrate. The amorphous structure of the anodized layer obtained in phosphate electrolyte might be one of the reasons for these electrochemical phenomena or excellent corrosion protectivity, and detailed analyses of conversion coatings should give additional information. The elements working in the sacrificial function and the changes in oxidation number, as well as the mechanism of the following formation of another protective layer, will hopefully be clarified in the future work. The regenerated films which consist of oxygen, magnesium, aluminum and phosphorus (Figs. 11, 12 and 13) are thought to be obtained by dissolution of the anodized layers and following formation of an insoluble or poorly soluble salt as magnesium phosphates ( $Mg_3(PO_4)_2 \cdot 4H_2O$ ,  $Mg_3(PO_4)_2 \cdot 8H_2O$ ) or magnesium hydrophosphates ( $MgHPO_4 \cdot 3H_2O$ ,  $MgHPO_4 \cdot 7H_2O$ ). When the formation rate of the above dense inert film surpasses that of magnesium hydroxide, corrosion which spoils the appearance of a product can be well suppressed. Although the films show some cracks in them, their adhesion to the substrates is better than that of magnesium hydroxide (Fig.9), and the front of each crack where the substrate is exposed can be covered successfully with the inert film mentioned above. Thus, the areas covered with the regenerated films are thought to avoid formation of magnesium



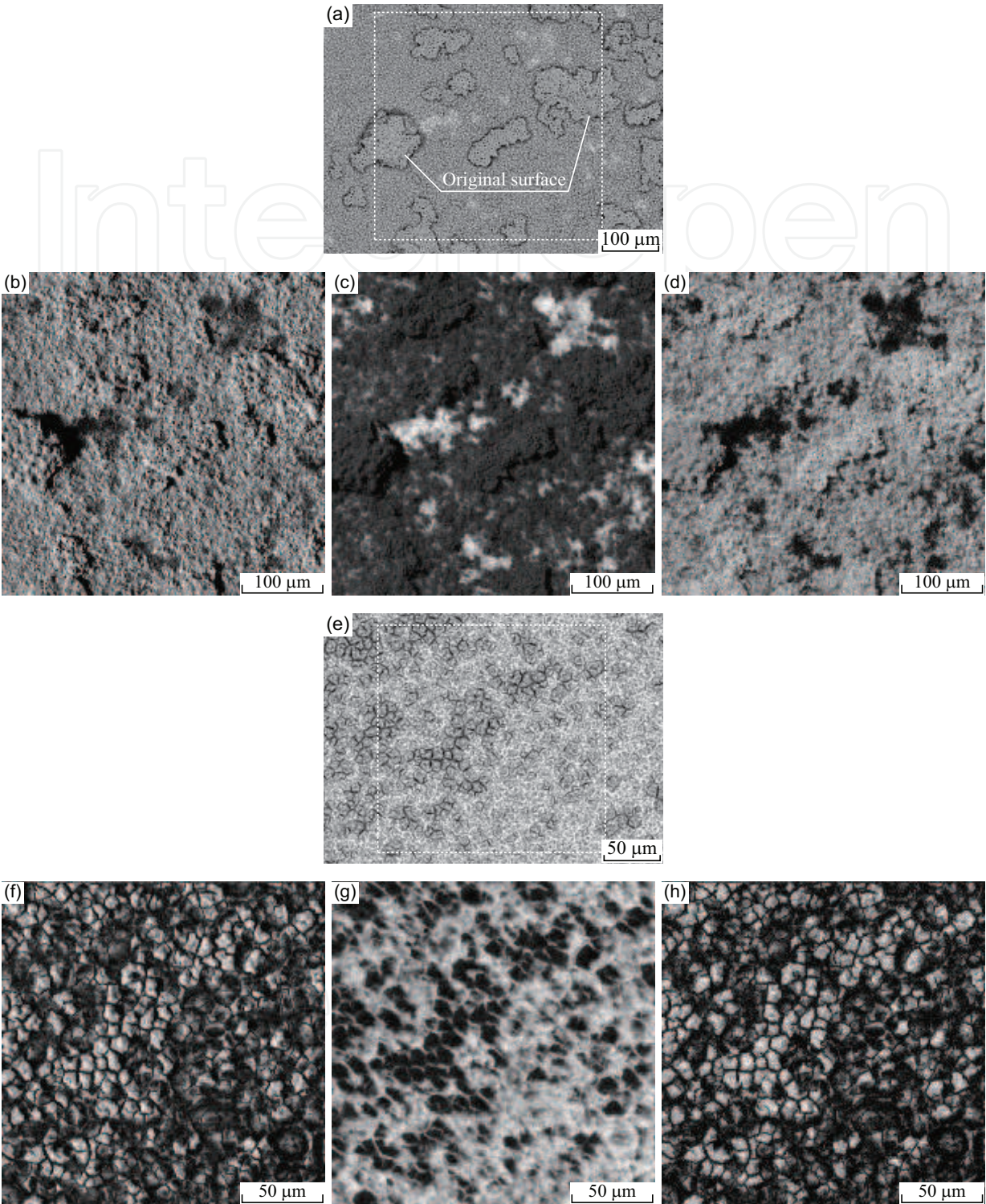


Fig. 14. Anodized surface of AZ91D-phosphate-10μm after salt spray test for (a)-(d) 346 ks and (e)-(h) 1990 ks ((a) Backscattered electron image, (b) Intensity map of O- $K\alpha$  characteristic X-ray in the dotted rectangular area of (a), (c) Mg- $K\alpha$ , (d) P- $K\alpha$ , (e) Backscattered electron image, (f) Intensity map of O- $K\alpha$  in the dotted rectangular area of (e), (g) Mg- $K\alpha$ , (h) P- $K\alpha$ ).

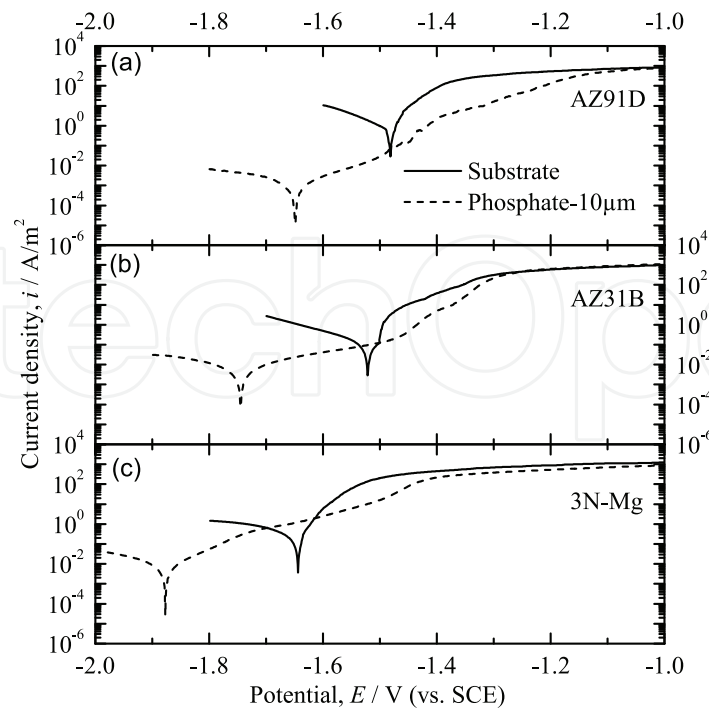


Fig. 15. Polarization curves of the raw and the anodized (phosphate) surfaces obtained by LSV in 5 mass% sodium chloride solution ((a) AZ91D, (b) AZ31B, (c) 3N-Mg, Sweep rate 1 mV/s).

hydroxide or visible corrosion as long as the original anodized layer exists on the surface and keeps dissolving slowly into the wet environment. Here, electrons generated by dissolution or oxidation of magnesium in the substrate are thought to be consumed by the reduction of hydrogen ion ( $2\text{H}^+ + 2\text{e}^- \rightarrow \text{H}_2$ ) which occurs near the anode sites. Since thickness of the regenerated film is the largest in the case of 3N-Mg and the second largest in the case of AZ31B, the formational rate of the film is thought to become larger for a substrate whose corrosion resistance is poorer. That is, the regenerated film is the

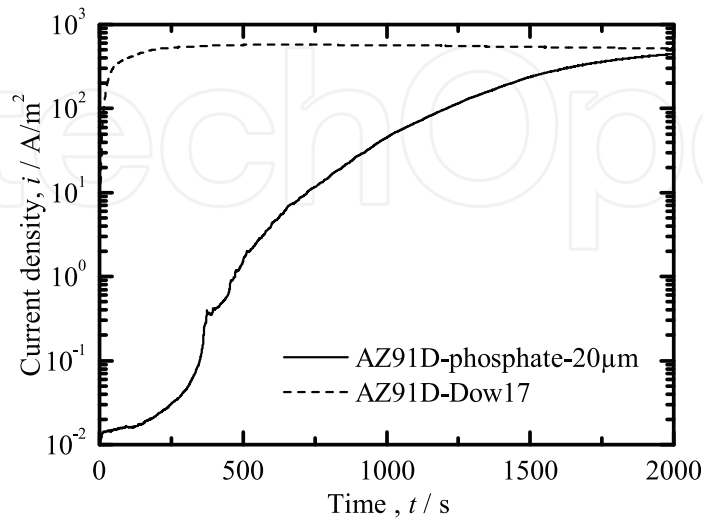


Fig. 16. Temporal change in current density on AZ91D-Dow17 and AZ91D-phosphate-20µm held at a constant potential of -1.4 V (vs. SCE) in 5 mass% sodium chloride solution.



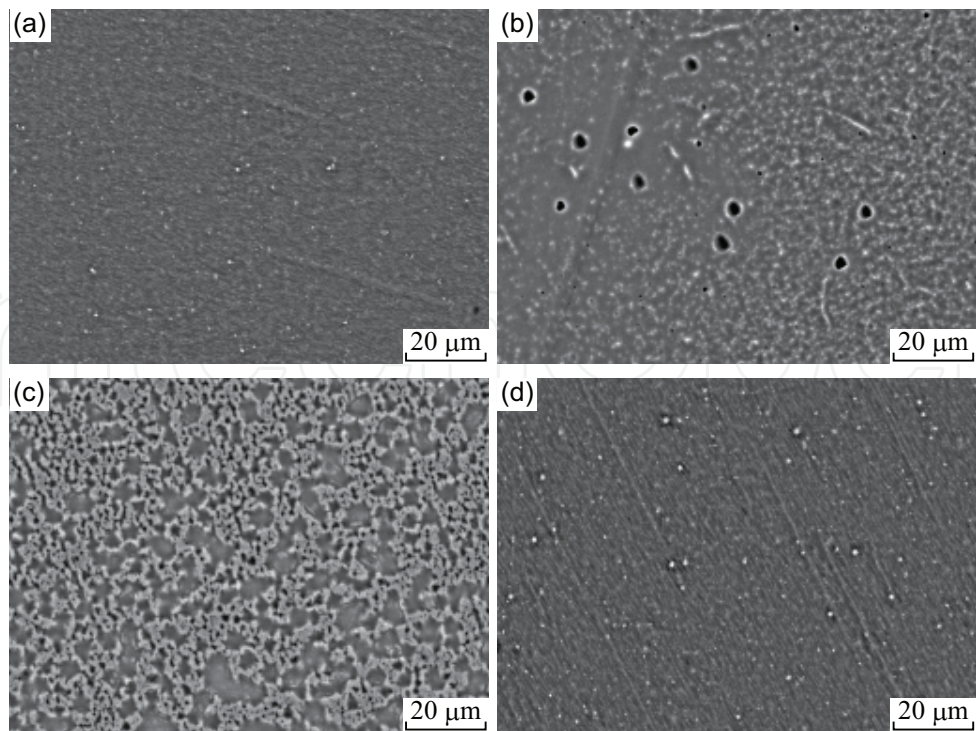


Fig. 17. Surface morphology of 3N-Mg after immersion into the trisodium phosphate solutions ((a) After pickling, (b) pH = 3, (c) pH = 7, (d) pH = 11).

result of reaction of substrate (magnesium) with dissolved chemical agents as phosphate ion ( $\text{PO}_4^{3-}$ ), hydrogen phosphate ion ( $\text{HPO}_4^{2-}$ ), dihydrogen phosphate ion ( $\text{H}_2\text{PO}_4^-$ ), or aqueous phosphoric acid ( $\text{H}_3\text{PO}_4$ ) at certain pH. From the point that a film is obtained at pH = 7 in the solution of trisodium phosphate (Fig. 17(c)) which can successfully cover the highly active surface of magnesium, the pH of the environment near the trench is supposedly  $\sim 7$  where hydrogen phosphate ion ( $\text{HPO}_4^{2-}$ ) and dihydrogen phosphate ion ( $\text{H}_2\text{PO}_4^-$ ) predominate. This is explained by setting pH = 7 ( $[\text{H}^+] = 10^{-7}$ ) for  $K_{a1} = [\text{H}^+][\text{H}_2\text{PO}_4^-]/[\text{H}_3\text{PO}_4] = 7.5 \times 10^{-3}$ ,  $K_{a2} = [\text{H}^+][\text{HPO}_4^{2-}]/[\text{H}_2\text{PO}_4^-] = 6.2 \times 10^{-8}$ ,  $K_{a3} = [\text{H}^+][\text{PO}_4^{3-}]/[\text{HPO}_4^{2-}] = 2.1 \times 10^{-13}$ . A schematic illustration of dissolution of the original anodized layer and regeneration of the protective film is shown in Fig. 18.

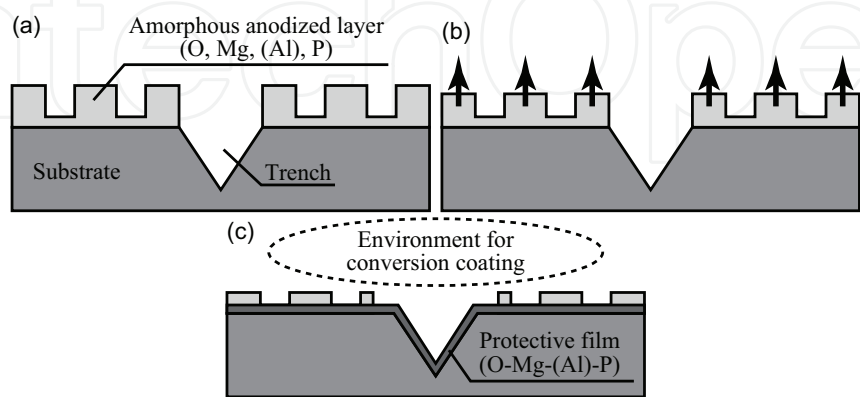


Fig. 18. Schematic illustration of the mechanism of corrosion protection during salt spray test ((a) before test, (b) dissolution of anodized layer, (c) formation of protective layer on the exposed areas of the substrate).

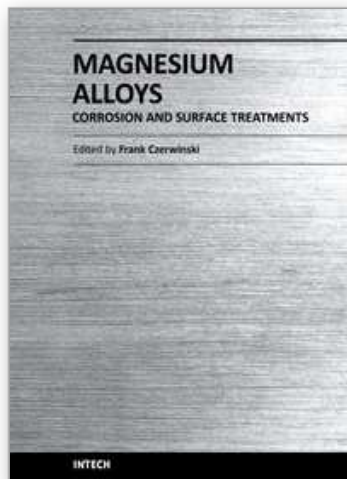
#### 4. Summary

In this chapter, microstructure of anodized layer on magnesium alloys and high-purity magnesium obtained by electrolysis in phosphate solution and corrosion protection by the anodized layers were discussed. The main results can be summarized as follows.

1. The anodized layers obtained in phosphate electrolyte consist of amorphous matrix and fine crystallites of spinel and magnesium oxide.
2. The anodized layers show sacrificial function in wet environment, while that in Dow17 shows barrier protection by passive film.
3. Corrosion protection by anodized layers formed in the phosphate electrolyte is based on electrochemically less nobleness of the original anodized layers whose dissolving rate is quite low. That is, ideal sacrificial function is provided on the substrates in terms of thermodynamics and kinetics.
4. Formation of another protective film on the areas where the original anodized layer is lost prevents substrates from bearing remarkable corrosion product of magnesium hydroxide.

#### 5. References

- (1981). Military Specifications and Standards (1981) MIL-M-45202C.
- (1998). American Society for Testing and Materials (1998) ASTM D 1732-67.
- Bansal, G. K. & Heuer, A. H. (1974). *Phil. Mag.* 24: 709–722.
- Barton, T. (1998). U.S. Pat. 5792335.
- Bonilla, F. A.; Berkani, A.; Liu, Y.; Skeldon, P.; Thompson, G. E.; Habazaki, H.; Shimizu, K.; John, C. & Stevens, K. (2002). *J. Electrochem. Soc.* 149: B4–B13.
- Cai, Q.; Wang, L.; Wei, B. & Liu, Q. (2006). *Surf. Coat. Tech.* 200: 3727–3733.
- Cole, G. S. (2003). *Mater. Sci. Forum* 419-422: 43–50.
- Company, T. D. C. (1956). GB Pat. 762195.
- Evangelides, H. (1955). U.S. Pat. 2723952.
- Hawke, D. & Albright, D. L. (1995). *Metal Fin.* 93: 34–38.
- Hino, M.; Murakami, K.; Hiramatsu, M.; Saijo, A. & Kanadani, T. (2007). *Mater. Sci. Forum* 539-543: 1691–1695.
- Hino, M.; Murakami, K.; Saijo, A. & Kanadani, T. (2008). *Mater. Trans.* 49: 924–930.
- Liang, J.; Guo, B.; Tian, J.; Liu, H.; Zhou, J.; Liu, W. & Xu, T. (2005). *Surf. Coat. Tech.* 199: 121–126.
- Mears, R. B. & Brown, C. D. (1945). *Corrosion – Nat. Assoc. of Corr. Eng.* 1: 113–118.
- Murakami, K.; Hino, M.; Hiramatsu, M.; Nakai, K.; Kobayashi, S.; Saijo, A. & Kanadani, T. (2007). *Mater. Trans.* 48: 3101–3108.
- Murakami, K.; Hino, M.; Hiramatsu, M.; Nakai, K.; Kobayashi, S.; Saijo, A. & Kanadani, T. (2008). *Mater. Trans.* 49: 1057–1064.
- Ono, S. & Masuko, N. (2003). *Mater. Sci. Forum* 419-422: 897–902.
- Osborn, E. F. (1953). *J. Am. Ceram. Soc.* 36: 147–151.
- Pourbaix, M. (1974). *Atlas of Electrochemical Equilibria in Aqueous Solutions*, National Association of Corrosion Engineers, Houston, Texas, USA.
- Saijo, A.; Hino, M.; Hiramatsu, M. & Kanadani, T. (2005). *Acta Metall. Sinica* 18: 411–415.
- Saijo, A.; Murakami, K.; Hino, M. & Kanadani, T. (2008). *Mater. Trans.* 49: 903–908.



## **Magnesium Alloys - Corrosion and Surface Treatments**

Edited by Frank Czerwinski

ISBN 978-953-307-972-1

Hard cover, 344 pages

**Publisher** InTech

**Published online** 14, January, 2011

**Published in print edition** January, 2011

A resistance of magnesium alloys to surface degradation is paramount for their applications in automotive, aerospace, consumer electronics and general-purpose markets. An emphasis of this book is on oxidation, corrosion and surface modifications, designed to enhance the alloy surface stability. It covers a nature of oxides grown at elevated temperatures and oxidation characteristics of selected alloys along with elements of general and electrochemical corrosion. Medical applications are considered that explore bio-compatibility of magnesium alloys. Also techniques of surface modifications, designed to improve not only corrosion resistance but also corrosion fatigue, wear and other behaviors, are described. The book represents a valuable resource for scientists and engineers from academia and industry.

### **How to reference**

In order to correctly reference this scholarly work, feel free to copy and paste the following:

Koji Murakami, Makoto Hino and Teruto Kanadani (2011). Anodization of Magnesium Alloys Using Phosphate Solution, *Magnesium Alloys - Corrosion and Surface Treatments*, Frank Czerwinski (Ed.), ISBN: 978-953-307-972-1, InTech, Available from: <http://www.intechopen.com/books/magnesium-alloys-corrosion-and-surface-treatments/anodization-of-magnesium-alloys-using-phosphate-solution>

**INTECH**  
open science | open minds

### **InTech Europe**

University Campus STeP Ri  
Slavka Krautzeka 83/A  
51000 Rijeka, Croatia  
Phone: +385 (51) 770 447  
Fax: +385 (51) 686 166  
[www.intechopen.com](http://www.intechopen.com)

### **InTech China**

Unit 405, Office Block, Hotel Equatorial Shanghai  
No.65, Yan An Road (West), Shanghai, 200040, China  
中国上海市延安西路65号上海国际贵都大饭店办公楼405单元  
Phone: +86-21-62489820  
Fax: +86-21-62489821



© 2011 The Author(s). Licensee IntechOpen. This chapter is distributed under the terms of the [Creative Commons Attribution-NonCommercial-ShareAlike-3.0 License](https://creativecommons.org/licenses/by-nc-sa/3.0/), which permits use, distribution and reproduction for non-commercial purposes, provided the original is properly cited and derivative works building on this content are distributed under the same license.

IntechOpen

IntechOpen